Applied Catalysis B: Environmental 307 (2022) 121152

Contents lists available at ScienceDirect

Applied Catalysis B: Environmental

journal homepage: www.elsevier.com/locate/apcatb

Visible light-driven H_2O_2 synthesis by a Cu_3BiS_3 photocathode via a photoelectrochemical indirect two-electron oxygen reduction reaction

Chao Chen [a,b], Miharu Yasugi [b], Lei Yu [a,*], Zhenyuan Teng [b,d,*], Teruhisa Ohno [b,c,**]

[a] School of Chemistry and Chemical Engineering, Yangzhou University, Yangzhou 225002, China
[b] Department of Applied Chemistry, Faculty of Engineering, Kyushu Institute of Technology, 1–1 Sensuicho, Tobata, Kitakyushu 804-8550, Japan
[c] Joint Laboratory of Yangzhou University, Kyushu Institute of Technology, Yangzhou University, 180 Si-Wang-Ting Road, Yangzhou 225002, China
[d] Research Initiative for Supra-Materials, Shinshu University, Nagano, 3808553, Japan

ARTICLE INFO

Keywords:
Cu_3BiS_3
Photocathode
Photoelectrochemical synthesis
O_2 reduction reaction
H_2O_2 production

ABSTRACT

In this study, a flat and uniform polycrystalline Cu_3BiS_3 (CBS) thin film was prepared on a molybdenum-coated glass (Mo-SLG) by spray pyrolysis deposition for generation of hydrogen peroxide (H_2O_2). The dense structure of the film promoted charge transmission, and the combination of the *p*-type CBS and *n*-type semiconductor In_2S_3 deposited by the chemical bath method improved the electron-hole separation efficiency, resulting in a significantly enhanced photocurrent. Deposition of Au nanoparticles reduced the required free energy for oxygen reduction reaction (ORR), improving the selectivity from O_2 to H_2O_2. The photoelectrochemical (PEC) synthesis proceeds by an indirect $2e^-$ ORR initial formation of superoxide, which is disproportionated to H_2O_2. In the presence of oxygen and visible light, Au-In_2S_3/CBS could be used to synthesize H_2O_2 (5.5 $mg{\cdot}L^{-1}{\cdot}h^{-1}{\cdot}cm^{-1}$) with good Faraday efficiency (71%). This study provided a practical strategy for designing a highly efficient photocathode to produce H_2O_2 based on improvement in electron-hole transmission efficiency and product selectivity.

1. Introduction

Hydrogen peroxide (H_2O_2) has received increasing attention as a product of artificial photosynthesis, a promising strategy for solar energy conversion [1–3]. Additionally, H_2O_2 has the advantage of high energy density and can be stored as an aqueous solution at normal temperature and pressure [4]. The development of H_2O_2 fuel cells (theoretical $V_{oc} = 1.1$ V, comparable to 1.23 V of H_2 fuel cells) has made H_2O_2 become a new ideal solar fuel [5,6]. Generally, there are two photocatalytic H_2O_2 production pathways, i.e., particulate photocatalytic (PC) and photoelectrochemical (PEC) systems. The PC system has the advantages of convenience and high profitability [7–10]. However, the oxidation reaction and reduction reaction on the surface of the catalyst proceed simultaneously, and thus excellent activity and selectivity for both oxygen reduction reaction (ORR) and water oxidation reaction (WOR) are needed [10]. Tada et al. reported a carbonate-modified surface Au nanoparticle-loaded rutile TiO_2 for ORR to generate H_2O_2. Unfortunately, HCOOH as a sacrificing electron donor was needed [11]. For the systems of photoelectrochemical cells, oxidation and reduction reactions occur on the photoanode and photocathode, respectively, i.e., the selectivity and activity for ORR and WOR can be separately improved. Studies on WOR generating H_2O_2 have mainly focused on the development of photoanode metal oxide materials [12]. Fuku et al. reported that a WO_3/$BiVO_4$ photoanode coated with a mesoporous Al_2O_3 layer could lead to excellent oxidative H_2O_2 generation at a selectivity of ca. 80% [13]. Yin et al. developed a $BiVO_4$ photoanode with surface oxygen vacancies that showed a photocurrent density of 4.32 $mA{\cdot}cm^{-2}$ at 1.23 vs. RHE [14]. However, H_2O_2 production via WOR by PEC systems is restricted by the high redox potential for H_2O_2 production via WOR (1.74 eV vs. RHE; Eq.1). Prevention of the decomposition of H_2O_2 at such high oxidation potential is difficult since H_2O_2 usually serves as an excellent hole scavenger and an intermediate reductant. In this case, accumulation of H_2O_2 is difficult in a PEC system that mainly relies on $2e^-$ WOR.

$$2H_2O + 2h^+ \rightarrow H_2O_2 + 2H^+ \quad E^0 = 1.76\ \text{eV}\ vs.\ RHE \tag{1}$$

$$O_2 + 2H^+ + 2e^- \rightarrow H_2O_2 \quad E^0 = 0.68\ \text{eV}\ vs.\ RHE \tag{2}$$

* Corresponding authors.
** Corresponding author at: Department of Applied Chemistry, Faculty of Engineering, Kyushu Institute of Technology, 1–1 Sensuicho, Tobata, Kitakyushu 804-8550, Japan.
E-mail addresses: yulei@yzu.edu.cn (L. Yu), zy.teng@foxmail.com (Z. Teng), tohno@che.kyutech.ac.jp (T. Ohno).

https://doi.org/10.1016/j.apcatb.2022.121152
Received 13 September 2021; Received in revised form 28 December 2021; Accepted 26 January 2022
Available online 29 January 2022

The use of a PEC system for boosting 2e⁻ ORR (0.68 eV vs. RHE; Eq. 2) is a promising strategy for H_2O_2 production. Up to now, only a few kinds of semiconductors have shown activity for PEC 2e⁻ ORR, most of which were organic materials that showed activity via a photosensitizer effect with dyes [15,16]. However, these photo-responsive dyes were often toxic. For example, the accumulation of porphyrin in the human body can lead to porphyria [17]. In addition, most of the processes for preparation of organic photosensitizers were complicated, thus increasing their preparation costs. Alternatively, inorganic materials have the advantage of high carrier mobility. Besides, their preparation steps are relatively simple, which reduces the manufacturing cost. However, the only successful inorganic *p*-type semiconductor system for photocatalytic H_2O_2 production was Gd-doped $CuBi_2O_4$/CuO. Unfortunately, this system required an electrolyte of 0.1 M KOH since the CuO coating could be easily decomposed under acidic and neutral conditions [18]. In this case, such strong alkaline conditions restricted the accumulation of H_2O_2 and limited the maximum concentration of H_2O_2. Furthermore, the O2p orbitals of metal oxides usually result in a deep valence band, thus leading to a large bandgap (2.2–3.5 eV) and an undesired light usage [19].

Copper-based sulfides, such as $CuInS_2$ [20–22], and Cu_2ZnSnS_4 [23,24], have attracted increasing attention for solar to chemical conversion efficiency due to their suitable bandgaps and high absorption coefficients ($>10^5$ cm^{-1}) [25]. Their S2p orbitals could enhance light absorption (bandgap of 1.1–2 eV) compared with metal oxide semiconductors with O2p orbitals [26]. Additionally, copper-based sulfides were not easily dissolved under acidic or neutral conditions. In this case, sulfides are promising inorganic materials for preparation of photocathodes for H_2O_2 production via 2e⁻ ORR [27,28]. Li et al. reported a particle-on-flower nanostructure Au-Cu_3BiS_3 for PEC HER [29]. They coated Au-Cu_3BiS_3 nanoparticles with a flower-like structure on ITO glass to prepare thin-film electrodes to obtain a larger specific surface area and more active sites. Spray pyrolysis deposition (SPD) and electrophoresis deposition (EPD) are both excellent methods for preparing thin films (details can be seen in Table S1). Previously, we prepared Cu_3BiS_3 (CBS) thin-film electrodes by using EPD for PEC H_2 evolution [30]. However, particles of different sizes resulted in an unsmooth and porous surface of the electrode after the electrophoresis process. The unsmooth surface usually resulted in a poor charge transfer between the interface of *p-n* junctions (CBS/In_2S_3), thus leading to unsatisfactory photocurrents. Additionally, the Pt surface of the previous system is not suitable for H_2O_2 production since Pt usually reduces the change of free energy (ΔG) of intermediates during HER 4e⁻ ORR reaction (usually resulting in a high selectivity for HER and 4e⁻ ORR) [31]. A promising PEC system would enable efficient charge transfer for high activity and have a desirable surface for good selectivity. Thus, seeking a practical strategy for CBS to achieve PEC H_2O_2 production is still of great importance.

In this study, an efficient cathode of In_2S_3/CBS was fabricated by the combination of simple spray pyrolysis deposition (SPD) on a molybdenum-coated glass (Mo-SLG) and chemical bath deposition (Scheme 1). The electrode photocurrent during H_2O_2 production increased 131 times than that without In_2S_3 modification, which is 3 times higher than that in our previous work in the same bias conditions (0.35 V vs. NHE). After the deposition of Au as a co-catalyst, H_2O_2 was obtained through an indirect 2e⁻ ORR at a rate of 5.5 $mg{\cdot}L^{-1}{\cdot}h^{-1}{\cdot}cm^{-1}$ with a Faraday efficiency of 71%. To the best of our knowledge, it is the first report of a sulfide-based photocathode for photoelectrochemical synthesis of H_2O_2. Furthermore, this work provides a practical strategy for designing a highly efficient CBS photocathode and is easily accessible for other inorganic photocathodes.

2. Experimental section

2.1. Chemicals

Unless otherwise stated, all of the chemicals used in the study were of analytical grade and used without further purification. All solutions were prepared by using ultra-pure water. $Bi(NO_3)_3{\cdot}5H_2O$, $Cu(NO_3)_2{\cdot}3H_2O$, S powder, $InCl_3{\cdot}4H_2O$ and nitric acid of analytical grade were purchased from Wako Pure Chemical Industries, Ltd., Japan. C_2H_5NS of analytical grade was purchased from Tokyo Chemical

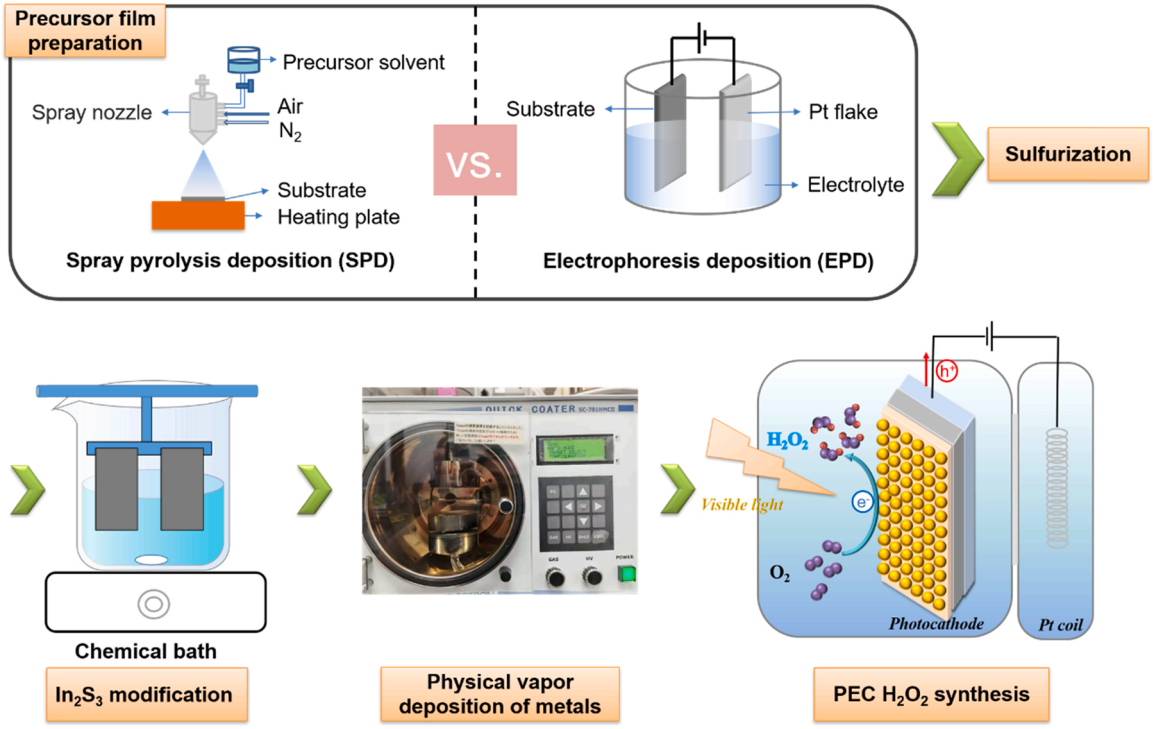

Scheme 1. Flow chart of Au-In_2S_3/Cu_3BiS_3 photocathode preparation.

Industry, Japan. Mo/SLG substrate was purchased from GEOMATEC Co. Ltd., Japan.

2.2. Fabrication of a Cu_3BiS_3 photocathode

In this study, typically, 0.9 M $Cu(NO_3)_2{\cdot}3H_2O$ (99.9%) and 0.3 M $Bi(NO_3)_3{\cdot}5H_2O$ (99.9%) were fully dissolved in 10% aqueous HNO_3 solution with stirring for 8 h and then the two solutions were mixed at a volume ratio of 1:1 to obtain the precursor solvent. The temperature of the reaction stage was controlled at 380 °C, and 5 mL of the precursor solvent was sprayed onto an Mo/SLG substrate (16 mm × 20 mm). The spraying time was controlled at 7 min. The precursor film was put into a glass tube together with 0.5 g of sulfur (99.9%), evacuated to 102 Pa, and then heated at 550 °C for 1 h. The heating rate was controlled at 5 °C/min. After cleaning with ammonia aqueous solution (25%) and ammonium sulfide (99.9%), the CBS photocathode was obtained.

2.3. Surface modification with an n-type In_2S_3 layer

An *n*-type In_2S_3 layer was formed by the chemical bath deposition method. During the process, 2.5 mmol of $InCl_3$ (99.9%), 10 mmol of thioacetamide (99.9%) and 0.6 mL of acetic acid (99.9%) were added into 100 mL of ultrapure water and stirred until they were completely dissolved. The electrode was immersed in the aqueous solution, and the bath was heated at 65 °C for 30 min. After that, the electrode was taken out, washed with ultrapure water, and then annealed at 100 °C for 20 min to obtain In_2S_3/CBS.

2.4. Deposition of Au

Au layers were sprayed onto the In_2S_3/CBS surfaces to a thickness of 2 nm using a programmable sputter coater (SC-701HMC II, Sanyu Electron Co.) with an Au disc target material (49*t0.5/4 N). Pt, Cu, Ag, and Ni layers were prepared by similar spray strategies.

2.5. Characterization of catalysts

The crystalline phases were characterized by using a powder X-ray diffraction (XRD) instrument (MiniFlex II, Rigaku Co.) with CuKα (λ = 1.5418 Å) radiation (cathode voltage: 30 kV, current: 15 mA). The absorption properties of an Au-In_2S_3/CBS electrode were measured using the diffuse reflection method with a UV−VIS spectrometer (UV-2600, Shimadzu Co.) attached to an integral sphere at room temperature. X-ray photoelectron spectroscopy (XPS) measurements were performed by using a Kratos AXIS Nova spectrometer (Shimadzu Co.) with a monochromatic Al Kα X-ray source. The binding energy was calibrated by taking the C1s peak of contaminant carbon as a reference at 284.6 eV. Raman spectroscopy measurements were performed with 532 nm excitation wavelength (NRS-5100, JASCO Co.).

2.6. Photoelectrochemical (PEC) measurement

The PEC performance of the CBS electrode was investigated in a three-electrode configuration by using a silver-silver chloride (Ag/AgCl) reference electrode and a Pt coil counter electrode. In order to avoid the influence of Pt^{2+}, an H-type electrolytic cell is used, and the Nafion™ membrane is used for isolation. The electrolytes were 0.1 M Eu^{3+}-containing aqueous solution, 0.1 M Na_2SO_4 solution (pH = 6) or 0.1 M phosphate buffer solution (pH = 7). All electrolytes were stirred and purged with N_2 gas or O_2 gas for 30 min before PEC measurement. In the case of 0.1 M phosphate buffer solution (pH = 7), the measured potential vs. Ag/AgCl was converted to RHE by Nernst's equation ($E_{RHE} = E_{Ag/AgCl} + 0.059\ pH + 0.197$). Linear sweep voltammetry and chronoamperometry measurements were carried out by an automatic polarization system (HSV-110, Hokuto Denko Co.) under visible light (420–800 nm) irradiation. The scan rate for the linear sweep voltammetry was 10 mV/s^{-1}. For details of the reaction device, please refer to the Supporting Information Fig. S1.

In the experiments of trapping superoxide radicals, the non-aqueous electrolyte was acetonitrile with 0.1 M tetra-n-butylammonium hexafluorophosphate ($TBAPF_6$) and 0.5 M acetic acid (CH_3COOH) dissolved. The Ag/Ag^+ electrode was used as a reference electrode and the electrolyte inside was acetonitrile with 0.1 M $TBAPF_6$ and 0.01 M $AgNO_3$ dissolved (Fig. S2). The Pt coil was used as a counter electrode. A Nafion™ membrane was used to separate anolytes and catholytes.

2.7. Analysis of products

H_2 gas was detected by an online gas chromatograph (GC) with a thermal conductivity detector (Agilent Technology Co. Micro GC) equipped with an MS-5A column. The amount of H_2O_2 was determined by a colorimetric method using PACKTEST (WAK-H_2O_2, KYORITSU CHEMICAL- CHECK Lab., Corp.) equipped with a digital PACKTEST spectrometer (ED723, GL Sciences Inc.).

3. Results and discussion

3.1. Comparison of electrodes prepared by electrophoretic deposition and spray pyrolysis deposition

The Cu_3BiS_3 (CBS) electrode was prepared via a two-step method. Firstly, a mixture solution of Bi and Cu was sprayed onto a Mo/SLG substrate. After formation of a mixed thin film of Bi_2O_3 and CuO by calcination at the high temperature of 550 °C, the as-prepared metal oxide film was sulfurized in a vacuum-sealed quartz tube. A CBS electrode was also prepared by EPD (EPD was used for preparation of Bi_2O_3 and CuO as a sulfurization precursor film.) for comparison. XRD spectra were used to verify the crystallinity of the as-prepared electrodes. As illustrated in XRD patterns (Fig. 1a), it was speculated that the main components of the precursor film prepared by SPD were amorphous Bi_2O_3 (JCPDS No. 50-1088) and CuO (JCPDS No. 48-1548). The film prepared by the EPD method showed an amorphous crystalline structure, which is unfavorable for further sulfurization to obtain a highly crystalline CBS electrode. On the other hand, the film prepared via SPD showed higher crystallinity. Typical diffractions of CuO (35.4°, 38.7° and 48.7°) and Bi_2O_3 were clearly observed, indicating a precursor film with high crystallinity. After the sulfurization process, the XRD patterns were obtained by measuring the films prepared by SPD and EPD (Fig. 1b) perfectly matched with the standard spectrum of CBS (JCPDS No. 43-1479), indicating that a CBS photocathode could be prepared by both methods. It is noteworthy that the full width at half maximum (FWHM, diffractions at 23.1°, 28.1°, 29.0°, 31.1° and 33.8°, details shown in Table S2) of the CBS electrode prepared by EPD was bigger than those by SPD, thus, a significantly higher crystallinity of the electrode prepared by SPD. Improved crystallinity of a photoelectrode usually results in an improved charge transfer in bulk phase, thus leading to a potentially higher photocurrent and more satisfactory activity.

The morphologies of the as-prepared CBS electrodes were characterized by scanning electron microscopy (SEM). An obvious difference was found in the structures of the CBS electrodes prepared by SPD and EPD. The precursor films prepared by EPD were composited by several large stacked microspheres (Fig. 2b). During the subsequent sulfurization process, these microspheres grew to form protruding particles, and obvious gaps between microspheres (enclosed by yellow dotted lines) were formed as shown in Fig. 2c and f. This untight film may significantly affect the charge transmission, thus resulting in unsatisfactory photoelectrochemical performance. The precursor film prepared by SPD (Fig. 2d) showed a sponge-like morphology. Although the surface is porous, the tiny particles of Bi_2O_3 and CuO formed a generally flat surface. During the further sulfurization process, a compact and uniform electrode with a thickness of ca. 2.1 μm was formed (Fig. 2e and g). This

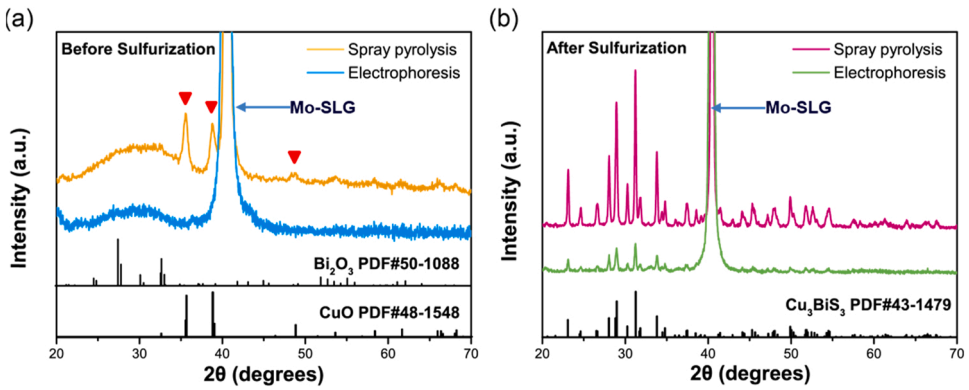

Fig. 1. XRD analysis of Cu_3BiS_3 electrodes prepared by SPD and EPD. (a) XRD analysis of photocathode films before sulfurization and (b) after sulfurization.

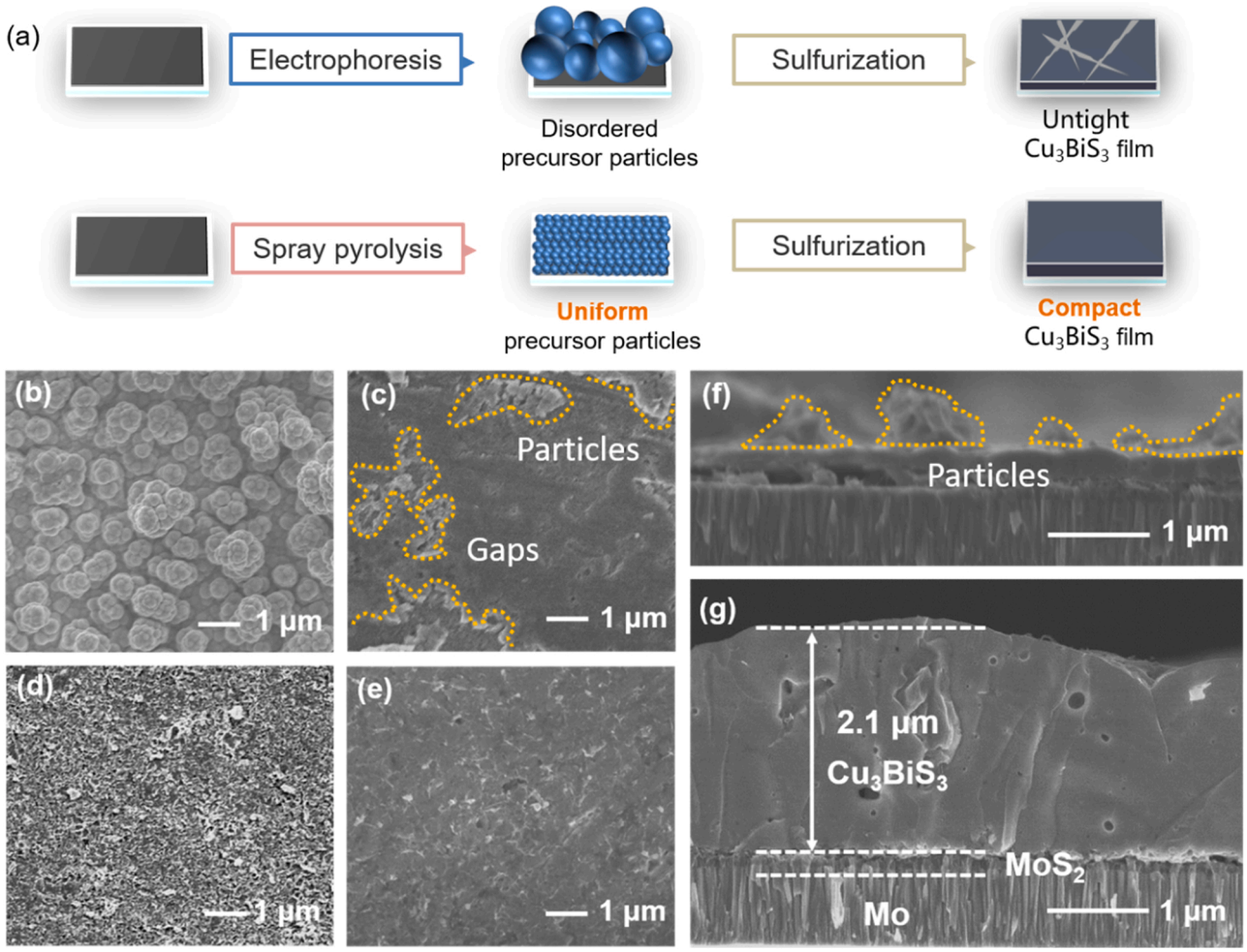

Fig. 2. SEM photographs of Cu_3BiS_3 electrodes prepared by SPD and EPD. (a) Schematic diagram for preparation for Cu_3BiS_3 photocathodes via (upper) electrophoresis and (lower) spray pyrolysis. (b) Top-view SEM photographs of photocathode films prepared by EPD before sulfurization and (c) after sulfurization and (d) those of photocathodes films prepared by SPD before sulfurization and (e) after sulfurization. (f) Cross-sectional SEM photograph of photocathode films prepared by EPD and (g) prepared by SPD after sulfurization.

is beneficial for the charge transfer between the Mo glass and the CBS layer, which may lead to a potentially large photocurrent. Additionally, the smooth surface of the CBS electrode is also beneficial for the charge transfer between the interface of Cu_3BiS_3 (*p*-type) and In_2S_3 (*n*-type). A satisfactory charge transfer between the *p-n* junctions also results in high photoelectrochemical performance of a photocathode.

UV–vis absorption spectra of CBS electrodes are shown in Fig. 3a. A similar absorption edge is observed in both samples prepared by EPD and SPD, indicating that the phase structure of CBS films has no change. In addition, the CBS electrode samples prepared by EPD had a higher background absorption at longer wavelengths ($\lambda > 700$ nm) than that of CBS electrodes samples prepared by SPD, and the band gap was also increased (1.62 eV vs. 1.58 eV) (Figs. 3b and S3), indicating a higher density of defects [32].

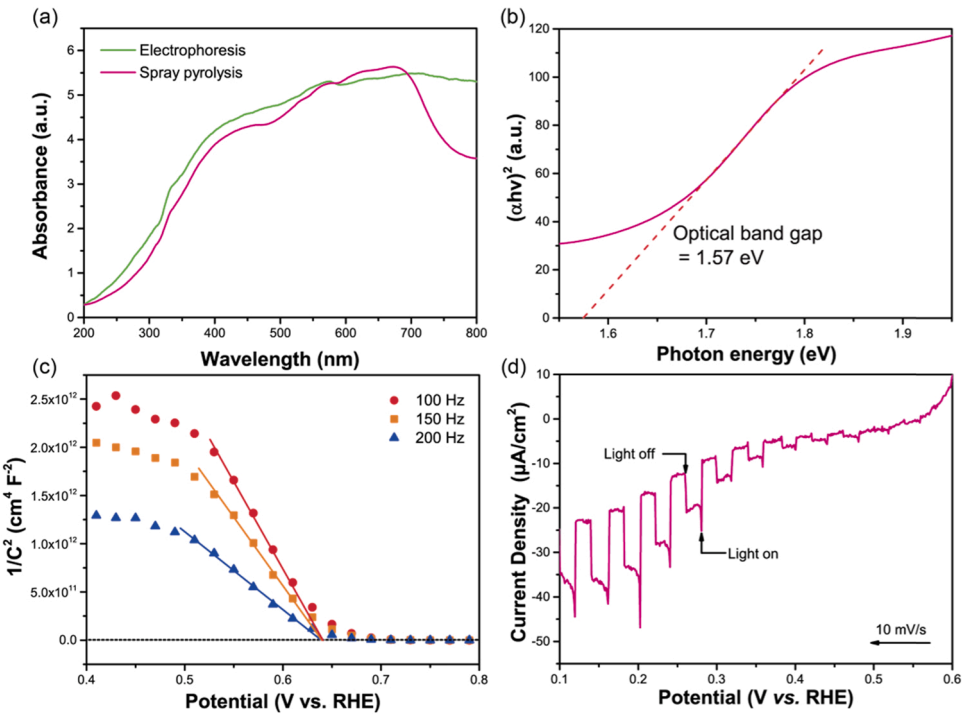

Fig. 3. Analysis of the band structures of Cu_3BiS_3 electrodes (a) UV-Vis spectra of Cu_3BiS_3 electrodes prepared by SPD and EPD. (b) Tauc plot for the Cu_3BiS_3 electrode prepared by SPD. (c) Mott–Schottky plots of the Cu_3BiS_3 electrode prepared by SPD. (d) Current–potential curve of the Cu_3BiS_3 electrode prepared by SPD in Ar-saturated $Eu(NO_3)_3$ solution (0.1 M, pH = 6) with chopped illumination from visible light (420–800 nm, 100 mW/cm^2).

To further analyze the band structure of as-prepared CBS electrodes, Mott–Schottky analysis was performed. The as-prepared CBS was confirmed to be a *p*-type semiconductor due to the negative slope in the Mott-Schottky plot (Fig. 3c) [33]. For *p*-type semiconductors, E_f is usually located near the valence band (VB). That is, the flat band potential is 0.1–0.3 eV lower than the VB potential [34]. As shown in Fig. 3c, E_{VB} was confirmed to be 0.44 eV (0.64 eV vs. RHE). Based on the above results, the E_{CB} of the CBS electrode prepared by SPD could be considered to be located at − 1.13 eV vs. RHE. As a comparison, the bandgap of the electrode prepared by EPD was calculated to be 1.62 eV, which has a slight blue-shift compared to that for the electrode prepared by SPD (1.58 eV) (Fig. S3). The difference between the band structures of electrodes prepared by EPD and SPD may be due to the compactness and thickness of the cathodic film [35].

To investigate selectivity of the CBS electrode for ORR, the current-potential response was investigated in an Ar-saturated electrolyte under illumination of a Xe lamp (USHIO UXL-500SX2, 420 < λ < 800 nm, 100 mW/cm^2). $Eu(NO_3)_3$ was added to the solution as an electron scavenger (Fig. 3d). The CBS electrode exhibited a cathodic photocurrent in response to irradiation of incident light, confirming that the prepared thin film was a *p*-type semiconductor [36]. The photocurrent increased when the electrode potential was shifted to a negative potential. Accordingly, a cathodic photocurrent could be observed at 0.4 V vs. RHE (pH=6), indicating that photoelectrochemical production occurred at the bias of ca. 0.7 V vs. NHE, and thus a 2e$^-$ ORR could occur on the surface of the electrode.

SPD was thought to be more advantageous than EPD for the preparation of a CBS electrode [37]. To compare the effects of the two preparation strategies on photoelectrochemical-catalytic activities, we fabricated a typical three-electrode cell by using CBS thin films (prepared by EPD or SPD) as working electrodes. Measurement of Tafel plots was carried out in a 0.1 M N_2-saturated Na_2SO_4 solution (0.1 M, pH = 6) at 25 °C. The Tafel curve is an intuitive basis for judging the activity of the catalyst. Generally, for HER and ORR, the smaller the Tafel slope means the better activity [38]. As shown in Fig. 4a, the linear regions of the Tafel plots were fitted well to the Tafel equation. Furthermore, the Tafel slope of the electrode prepared by SPD (79 mV dec^{-1}) was smaller than that of the electrode prepared by EPD (137 mV dec^{-1}). This may be

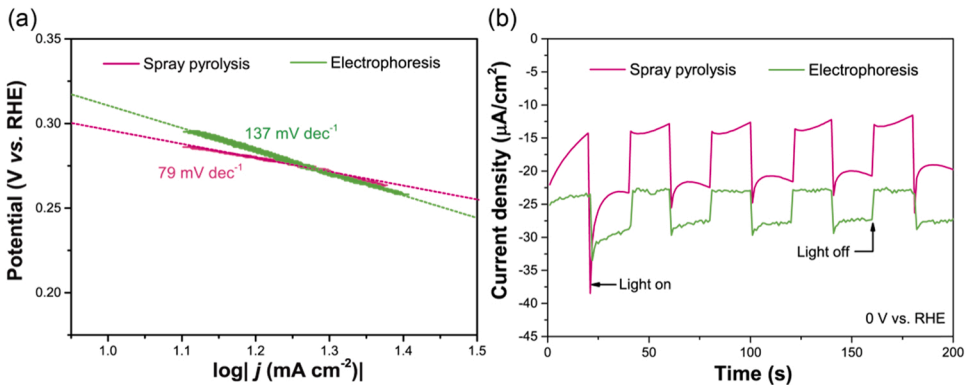

Fig. 4. Comparison of the photoactivity of electrodes prepared by electrophoresis and spray pyrolysis deposition. (a) Tafel plots of CBS films made by the spray pyrolysis deposition (pink) and the electrophoresis deposition (green) with their associated linear fittings (dashed lines) in Na_2SO_4 solution (0.1 M, pH = 6). (b) Time courses of the photocurrents of CBS electrodes made by the spray pyrolysis deposition (pink) and the electrophoresis deposition (green) in Ar-saturated $Eu(NO_3)_3$ solution (0.1 M, pH = 6) with visible light (420–800 nm, 100 mW/cm^2) irradiation under a potentiostatic condition at 0 V vs. V_{RHE}. (For interpretation of the references to color in this figure legend, the reader is referred to the web version of this article.)

attributable to the greater density of the thin film prepared by SPD, which accelerates carrier transfer. Under the same conditions, the photocurrent of the denser film increased ca. 1.5 times than the untight film prepared by EPD and the dark current was also reduced due to the disappearance of small particles on the surface (Fig. 4b). In addition, we conducted a comparative experiment and found that H_2O_2 could not be generated without photoirradiation, indicating that the electrode is undergoing a self-reduction reaction under dark current (Fig. S4). From the perspective of solar-to-chemical energetic conversion, the CBS electrode prepared by SPD was better than that prepared by EPD.

3.2. Modification with In_2S_3 for formation of p-n junctions

In order to improve the responsiveness of the CBS electrode to light, an *n*-type semiconductor could be used to modify the electrode for forming *p-n* junctions, a well-known strategy for improving the responsiveness to light by increasing the separation efficiency of electrons and holes [39]. In the previous work, the best photo-response could be obtained when In_2S_3 was selected for modification [40]. As shown in Fig. S5 in Supplementary Material, In_2S_3 was uniformly attached to the surface of the CBS electrode, which showed a lamellar flower-like structure. According to the SEM cross-sectional view, the thickness of In_2S_3 was ca. 130 nm. Furthermore, the noble metal deposition improved the photoelectric performance and acted as a protective layer for the *p*-type layer electrodes. The distribution of the Au, In_2S_3, CBS and Mo-SLG were clarified by the SEM image and corresponding mapping of the section of the as-prepared electrode (Fig. S6 and S7). The elemental compositions and the chemical states of the elements were further verified by XPS analysis (Fig. S8). UV–vis spectra showed that the CBS, In_2S_3/CBS and Au-In_2S_3/CBS electrodes performed the absorption of visible light (Fig. S9).

Fig. 5a shows linear sweep voltammograms (LSV) of Au-CBS, In_2S_3/CBS and Au-In_2S_3/CBS in O_2-bubbling phosphate buffer electrolyte (0.1 M, pH = 7) under chopped illumination from visible light (420–800 nm, 100 mW/cm^2). By blocking the light source once every 2 s, the current generated by the light irradiation was illustrated directly. When an In_2S_3 buffer layer was used to modify the CBS electrode, the photocurrent of the Au-In_2S_3/CBS electrode became the highest at ca. -125 μAcm^{-2} under the base potential of +0.4 V vs. RHE. Compared with the electrode that was not modified with In_2S_3 (Au-CBS) under the same bias potential, the photocurrent of Au-In_2S_3/CBS electrode prepared by SPD was significantly increased by 131 times. Nevertheless, the photocurrent of the electrode (Au-In_2S_3/CBS) prepared by EPD increased only ca. 5 times than that of Au-CBS under same condition according to our previous study [30]. This result may be attributed to the smooth CBS electrode surface that made the charge transfer at the interface between the two semiconductors easier, resulting in a larger photocurrent.

Electrochemical impedance spectroscopy (EIS) of the samples were performed in a phosphate buffer electrolyte (0.1 M, pH = 7) with visible light (420–800 nm, 100 mW/cm^2) irradiation. The exchange of charge carriers between the catalyst and the electrolyte at the interface is generally called the charge transfer process. The smaller semicircle in the Nyquist diagram indicates better charge transfer kinetics. With the modification of In_2S_3, the charge transfer resistance of CBS electrode decreased obviously, and this value even further decreased after the modification of Au nanoparticles (Fig. 5b). The results were in line with the conclusion of the previous LSV test. The increase in the charge transfer rate during the PEC process can be manifested as an increase in the photocurrent.

3.3. Optimization of the co-catalytic layer for H_2O_2 production

To investigate the optimized co-catalyst for the as-prepared electrode, several metals were loaded on In_2S_3/CBS electrodes. The activities of the as-prepared metal-modified In_2S_3/CBS electrodes were compared by measuring the photocurrents. The oxygen reduction reaction was carried out in an O_2-saturated phosphate buffer electrolyte (0.1 M, pH = 7) with visible light (420–800 nm, 100 mW/cm^2) irradiation under a potentiostatic condition at +0.4 V vs. V_{RHE}. The concentration of H_2O_2 produced by the Au-loaded electrode within one hour was 1.5 mg/L and a Faraday efficiency of ca. 64% was obtained, indicating an obvious advantage over other metal-loaded and non-loaded electrodes (Fig. 6). It is worth mentioning that the photocathodic compartment was gas-proof, which means the Au-loaded In_2S_3/CBS electrode showed selectivity for 2e$^-$ ORR since H_2 was not detected. The high selectivity may be due to the high activity of Au nanoparticles for ORR. The critical step was the formation of O-Au bonds with a corresponding decrease in the activation energy of molecular oxygen [41].

The amounts of produced H_2O_2 over time and the corresponding changes in Faraday efficiency were investigated to estimate the performance of the electrode (Figs. S10 and S11). Under the condition of O_2 bubbling, the amount of generated H_2O_2 was larger than that under the O_2-saturated condition (Figs. 7a and S12). After visible light irradiation for one hour, the concentration of H_2O_2 reached 5.5 mg/L, corresponding to a Faraday efficiency of 71%. Moreover, Faraday efficiency remained almost constant with elapse of time. We are convinced that the use of Au-In_2S_3/Cu_3BiS_3 to generate H_2O_2 is a pioneering work because the previously electrodes with PEC ORR activity are mostly organic compounds such as polymers or dyes. Compared with the advanced photocathode materials reported in recent years, Au-In_2S_3/Cu_3BiS_3 electrodes can provide a competitive level of H_2O_2 production (details could be seen in Table S3). Li et al. reported the highest rate of stable and continuous generation of hydrogen peroxide using photocathodes made by pTTh. However, the cost of precursor for preparing the electrode was extremely high (26200 yen/g). Gd-doped $CuBi_2O_4$/CuO electrode reported by Z. Li et al. could generate 1.3 mmol of H_2O_2 within 30 min. Unfortunately, this system required an electrolyte of 0.1 M KOH since

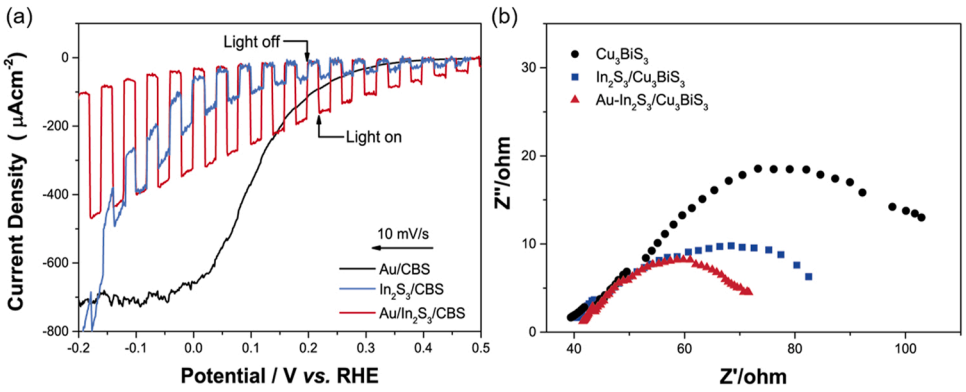

Fig. 5. Comparison of Cu_3BiS_3 electrodes with and without modification. (a) Linear sweep voltammograms of Au-Cu_3BiS_3, In_2S_3/Cu_3BiS_3 and Au-In_2S_3/Cu_3BiS_3 electrodes in O_2-bubbling phosphate buffer electrolyte (0.1 M, pH = 7) under chopped illumination from visible light (420–800 nm, 100 mW/cm^2) irradiation. (b) Nyquist plots of Cu_3BiS_3, In_2S_3/Cu_3BiS_3 and Au-In_2S_3/Cu_3BiS_3 in a phosphate buffer electrolyte (0.1 M, pH = 7) with visible light (420–800 nm, 100 mW/cm^2) irradiation. (For interpretation of the references to color in this figure legend, the reader is referred to the web version of this article.)

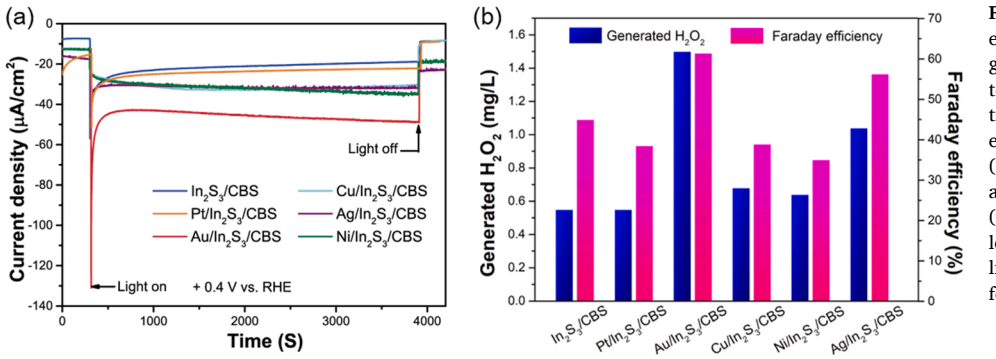

Fig. 6. Comparison of the activities of Cu_3BiS_3 electrodes with different loading metals for generating H_2O_2. (a) Time courses of the photocurrents of metal-loaded In_2S_3/Cu_3BiS_3 electrodes in an O_2-saturated phosphate buffer electrolyte (0.1 M, pH = 7) with visible light (420–800 nm, 100 mW/cm^2) irradiation under a potentiostatic condition at +0.4 V vs. V_{RHE}. (b) Amounts of generated H_2O_2 by metal-loaded In_2S_3/Cu_3BiS_3 electrodes with visible light (420–800 nm, 100 mW/cm^2) irradiation for 1 h and corresponding Faraday efficiencies.

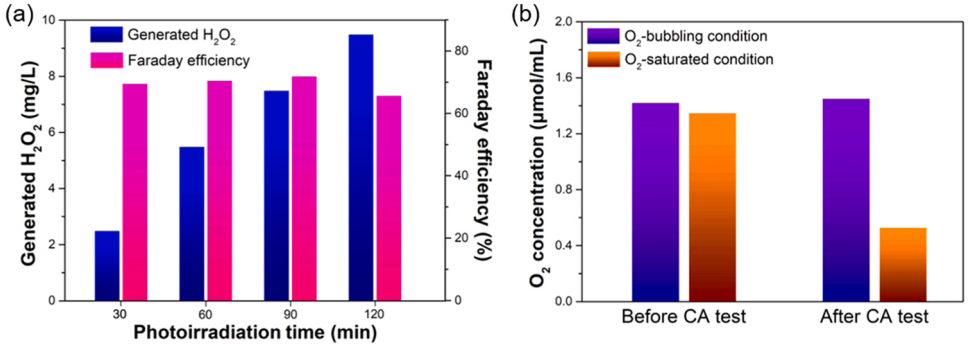

Fig. 7. Amounts of H_2O_2 produced as a function of photoirradiation time and effect of O_2 concentration. (a) H_2O_2 generated by the Au-In_2S_3/Cu_3BiS_3 electrode in an O_2-bubbling phosphate buffer electrolyte (0.1 M, pH = 7) under a potentiostatic condition at + 0.4 V_{RHE} with visible light (420–800 nm, 100 mW/cm^2) irradiation and corresponding Faraday efficiency. (b) O_2 concentrations before and after a 1 h CA test under O_2-bubbling and O_2-saturated conditions.

the CuO coating could be easily decomposed under acidic and neutral conditions. In this case, such strong alkaline conditions restricted the accumulation of H_2O_2. Therefore, developing a relatively-stable and cost-efficient inorganic photocathode for efficient H_2O_2 production is still of great urgent. Au-In_2S_3/Cu_3BiS_3 could photoelectrochemically generate H_2O_2 in the acidic/neutral condition. The stability is also significantly higher than other inorganic electrodes for PEC production of H_2O_2. Additionally, this Au-In_2S_3/Cu_3BiS_3 electrode is cost-efficient and highly selective, which could inspire other researchers to further develop efficient PEC systems for H_2O_2 production.

The difference between activities may be due to the changes of O_2 concentrations in the aqueous electrolyte over time. Under the gas-proof condition (O_2-saturated), O_2 was continuously converted to H_2O_2, resulting in a decrease in O_2 concentration in the cathode compartment. Under the condition of O_2-bubbling, the O_2 concentration remains constant, and the interaction between the electrode surface and O_2 will be more efficient. To prove this assumption, O_2 concentrations before and after a 1 h CA test under the two conditions were measured by Micro-GC (Fig. 7b), and the results showed that the O_2 concentration after the reaction under the gas-proof condition (O_2-saturated) was only 1/3 of that under the condition of O_2 bubbling. Furthermore, the oxygen bubbling may accelerate the electrode surface's mass transfer process [42]. Since the superoxide radical could be more uniformly dispersed in the electrolyte, it caused minor damage to the electrodes so that the system could maintain a higher Faraday efficiency. Moreover, we performed XRD analysis and ICP-AES analysis to compare the CBS electrodes before and after the reaction, and the species of the CBS electrodes did not change (Figs. S13 and S14). Subsequently, three cycle experiments (two hours each time) for H_2O_2 generation were carried out, and the Faraday efficiency could be maintained at 84.5% of the first time (Fig. S15). The results indicated that the as-prepared Au-In_2S_3/CBS electrode showed satisfactory stability for PEC production of H_2O_2.

3.4. Photoelectrocatalytic mechanism analysis

In order to further confirm the reaction mechanism, we performed a superoxide radical capture experiment based on the nucleophilic substitution reactions between acyl halides and superoxide. In an aqueous solution, superoxide radicals quickly react with protons to generate H_2O_2 and O_2. Therefore, the superoxide radical capture experiment was carried out in a non-aqueous solution with benzoyl chloride (BzCl) as a model compound to react with photoelectrochemically generated superoxide radical anion ($^{\bullet}O_2^-$) (Fig. 8a). As shown in Fig. 8b, the amount of H_2O_2 in the non-aqueous solution and the corresponding Faraday efficiency both decreased. This may be due to the fact that the electrode is more hydrophilic as an inorganic sulfide. After adding BzCl, the amount of H_2O_2 generated decreased obviously (Fig. 8c), indicating that $^{\bullet}O_2^-$, as an important intermediate product, was captured by BzCl and could not be further reduced to H_2O_2 [43]. Therefore, the reaction mechanism can be briefly described as photoexcited electrons on CBS reducing O_2 to $^{\bullet}O_2^-$ and then further being disproportionated to generate H_2O_2. The above conclusion is similar to previous works on 2e$^-$ ORR to generate H_2O_2 [44–46]. In addition, the single interfacial electron transfer simplified the PEC system and minimized the opportunities for charge recombination [47].

The process of photoelectrochemical generation of H_2O_2 is summarized in Fig. 8d. A compact and uniform CBS and In_2S_3 layer formed a typical type II heterojunction structure, which helped the separation and transfer of charge. Au nanoparticles worked as a co-catalyst to further enhance the charge transfer and selectivity of O_2/H_2O_2 reduction. Photon absorption caused both semiconductors to be excited (step 1). The holes transferred (HT) from In_2S_3 to CBS and then further transferred to the photoanode instead of recombining with the electrons (step 2). As a result, electrons were transferred (ET) from CBS to Au nanoparticles and then further reduced O_2 to form $^{\bullet}O_2^-$ (step 3), which could be easily disproportionated in water to generate H_2O_2. Thus, we have

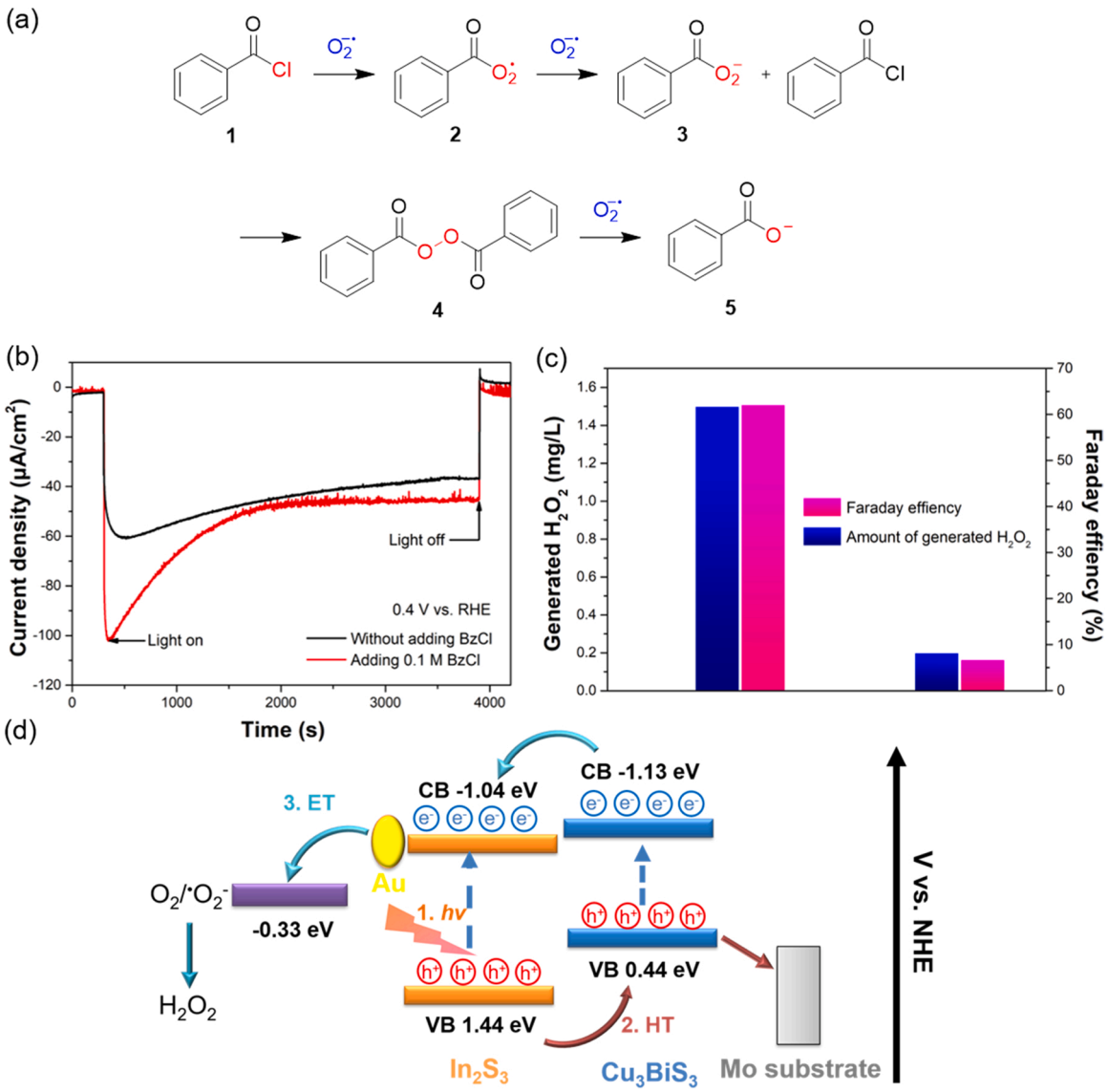

Fig. 8. Superoxide radical capture experiment and speculated reaction mechanism. (a) Proposed reactions between benzoyl chloride and superoxide radical anions. (b) CA test for adding BzCl (red line) and without adding BzCl (blue line). Time courses of the photocurrent of Au-In_2S_3/CBS electrodes in an O_2-bubbling non-aqueous electrolyte with visible light (420–800 nm, 100 mW/cm^2) irradiation under a potentiostatic condition at +0.4 V vs. V_{RHE}. (c) Amounts of H_2O_2 generated by Au-In_2S_3/CBS electrodes under the condition of addition or without no addition of BzCl with visible light (420–800 nm, 100 mW/cm^2) irradiation for 1 h and corresponding Faraday efficiencies. (d) Energy diagram for Au-In_2S_3/CBS electrodes depicting the process of H_2O_2 formation. (For interpretation of the references to color in this figure legend, the reader is referred to the web version of this article.)

constructed a photoelectrode activity-selectivity improvement strategy. Firstly, the film prepared by the SPD was excellent in denseness, which resulted in faster charge transmission and 1.5 times increased photocurrent than that of the films prepared by EPD. Secondly, the *p-n* heterojunction between the *p*-type semiconductor CBS and the *n*-type semiconductor In_2S_3 further promoted charge separation. In this step, the smooth CBS electrode surface will play an important role to improve the charge transfer at the interface between the two semiconductors. The tight combination of *p*-type and *n*-type semiconductors increased the photocurrent by 131 times than before In_2S_3 modification. Thirdly, the deposition of Au nanoparticles reduced the free energy required for ORR, improving the selectivity of O_2 to H_2O_2. Compared with the electrode without Au deposition, the rate of H_2O_2 generation is increased ca. 3 times.

4. Conclusions

In summary, in situ photoelectrochemical synthesis of H_2O_2 was achieved in this study for the first time by using an inorganic sulphide photocathode under visible light irradiation. Under the condition of visible light irradiation, the Au-loaded In_2S_3/CBS electrode could produce H_2O_2 at a rate of 5.5 mg·L^{-1}·h^{-1}·cm^{-1} with good Faraday efficiency. The PEC pathway can be briefly described as photo-excited electrons on CBS reducing O_2 to $^{\bullet}O_2^-$ and then further being disproportionated to generate H_2O_2. Although superoxide radicals could cause some damage to the surface of the electrode, they minimize the opportunities for charge recombination. Compared with the traditional dye-sensitized photocathode, this study provided a practical strategy for designing a highly efficient inorganic photocathode for producing H_2O_2 and will evoke more interest in ORR via a PEC system.

CRediT authorship contribution statement

Chao Chen: Conceptualization, Methodology, Investigation, Data curation, Formal analysis, Writing – original draft. **Miharu Yasugi:** Investigation, Formal analysis, Data curation. **Lei Yu:** Writing – review & editing, Funding acquisition. **Zhengyuan Teng:** Conceptualization, Writing – review & editing. **Teruhisa Ohno:** Conceptualization, Writing – review & editing, Funding acquisition, Data curation.

Associated Contents

Supporting Information is available from the Publications online version or from the authors.

Declaration of Competing Interest

The authors declare that they have no known competing financial interests or personal relationships that could have appeared to influence the work reported in this paper.

Acknowledgements

The authors acknowledge the financial support of Yangzhou University International Academic Exchange Fund (YZUIAEF201901004), Jiangsu Provincial Six Talent Peaks Project (No. XCL-090), Priority Academic Program Development of Jiangsu Higher Education Institutions (PAPD) and Japan Society for the Promotion of Science (JSPS), Grant-in-Aid for Scientific Research (B) (20H02847).

Appendix A. Supporting information

Supplementary data associated with this article can be found in the online version at doi:10.1016/j.apcatb.2022.121152.

References

[1] S. Fukuzumi, Production of liquid solar fuels and their use in fuel cells, Joule 1 (2017) 689–738, https://doi.org/10.1016/j.joule.2017.07.007.
[2] S. Fukuzumi, Y.M. Lee, W. Nam, Solar-driven production of hydrogen peroxide from water and dioxygen, Chem 24 (2018) 5016–5031, https://doi.org/10.1002/chem.201704512.
[3] S. Siahrostami, S.J. Villegas, A.H.B. Mostaghimi, S. Back, A.B. Farimani, H. Wang, K.A. Persson, J. Montoya, A review on challenges and successes in atomic-scale design of catalysts for electrochemical synthesis of hydrogen peroxide, ACS Catal. 10 (2020) 7495–7511, https://doi.org/10.1021/acscatal.0c01641.
[4] X. Zeng, Y. Liu, X. Hu, X. Zhang, Photoredox catalysis over semiconductors for light-driven hydrogen peroxide production, Green Chem. 23 (2021) 1466–1494, https://doi.org/10.1039/D0GC04236F.
[5] S.A. Mousavi Shaegh, N.-T. Nguyen, S.M. Mousavi Ehteshami, S.H. Chan, A membraneless hydrogen peroxidefuel cell using prussian blue as cathode material, Energy Environ. Sci. 5 (2012) 8225–8228, https://doi.org/10.1039/C2EE21806B.
[6] Y. Yamada, M. Yoneda, S. Fukuzumi, High and robust performance of H_2O_2 fuel cells in the presence of scandium ion, Energy Environ. Sci. 8 (2015) 1698–1701, https://doi.org/10.1039/C5EE00748H.
[7] M. Xiao, Z. Wang, M. Lyu, B. Luo, S. Wang, G. Liu, H.M. Cheng, L. Wang, Hollow nanostructures for photocatalysis: advantages and challenges, Adv. Mater. 31 (2019), 1801369, https://doi.org/10.1002/adma.201801369.
[8] Z. Teng, H. Lv, C. Wang, H. Xue, H. Pang, G. Wang, Bandgap engineering of ultrathin graphene-like carbon nitride nanosheets with controllable oxygenous functionalization, Carbon 113 (2017) 63–75, https://doi.org/10.1016/j.carbon.2016.11.030.
[9] Z. Teng, W. Cai, W. Sim, Q. Zhang, C. Wang, C. Su, T. Ohno, Photoexcited single metal atom catalysts for heterogeneous photocatalytic H_2O_2 production: pragmatic guidelines for predicting charge separation, Appl. Catal. B Environ. 282 (2021), 119589, https://doi.org/10.1016/j.apcatb.2020.119589.
[10] Z. Teng, Q. Zhang, H. Yang, K. Kato, W. Yang, Y. Lu, S. Liu, C. Wang, A. Yamakata, C. Su, B. Liu, T. Ohno, Atomically dispersed antimony on carbon nitride for the artificial photosynthesis of hydrogen peroxide, Nat. Catal. 4 (2021) 374–384, https://doi.org/10.1038/s41929-021-00605-1.
[11] M. Teranishi, R. Hoshino, S. Naya, H. Tada, Gold-nanoparticle-loaded carbonate-modified titanium(IV) oxide surface: visible-light-driven formation of hydrogen peroxide from oxygen, Angew. Chem., Int. Ed. 55 (2016) 12773–12777, https://doi.org/10.1002/anie.201606734.
[12] J. Liu, Y. Zou, B. Jin, K. Zhang, J.H. Park, Hydrogen peroxide production from solar water oxidation, ACS Energy Lett. 4 (2019) 3018–3027, https://doi.org/10.1021/acsenergylett.9b02199.
[13] K. Fuku, Y. Miyase, Y. Miseki, T. Gunji, K. Sayama, WO_3/$BiVO_4$ photoanode coated with mesoporous Al_2O_3 layer for oxidative production of hydrogen peroxide from water with high selectivity, RSC Adv. 7 (2017) 47619–47623, https://doi.org/10.1039/C7RA09693C.
[14] S. Jin, X. Ma, J. Pan, C. Zhu, S.E. Saji, J. Hua, X. Xu, L. Sun, Z. Yin, Oxygen vacancies activating surface reactivity to favor charge separation and transfer in nanoporous $BiVO_4$ photoanodes, Appl. Catal. B Environ. 281 (2021), 119477, https://doi.org/10.1016/j.apcatb.2020.119477.
[15] J. Sun, Y. Yu, A.E. Curtze, X. Liang, Y. Wu, Dye-sensitized photocathodes for oxygen reduction: efficient H_2O_2 production and aprotic redox reactions, Chem. Sci. 10 (2019) 5519–5527, https://doi.org/10.1039/C9SC01626K.
[16] W. Fan, B. Zhang, X. Wang, W. Ma, D. Li, Z. Wang, M. Dupuis, J. Shi, S. Liao, C. Li, Efficient hydrogen peroxide synthesis by metal-free polyterthiophene via photoelectrocatalytic dioxygen reduction, Energy Environ. Sci. 13 (2020) 238–245, https://doi.org/10.1039/C9EE02247C.
[17] H. Thadani, A. Deacon, T. Peters, Diagnosis and management of porphyria, BMJ 320 (2000) 1647–1651, https://doi.org/10.1136/bmj.320.7250.1647.
[18] Z. Li, Q. Xu, F. Gou, B. He, W. Chen, W. Zheng, X. Jiang, K. Chen, C. Qi, D. Ma, Gd-doped $CuBi_2O_4$/CuO heterojunction film photocathodes for photoelectrochemical H_2O_2 production through oxygen reduction, Nano Res. (2021), https://doi.org/10.1007/s12274-021-3638-y.
[19] Y. Xu, Schoonen, A.A. Martin, The absolute energy positions of conduction and valence bands of selected semiconducting minerals, Am. Mineral. 85 (2000) 543–556, https://doi.org/10.2138/am-2000-0416.
[20] M. Li, R. Zhao, Y. Su, J. Hu, Z. Yang, Y. Zhang, Synthesis of $CuInS_2$ nanowire arrays via solution transformation of Cu_2S self-template for enhanced photoelectrochemical performance, Appl. Catal. B Environ. 203 (2017) 715–724, https://doi.org/10.1016/j.apcatb.2016.10.051.
[21] F. Xu, J. Zhang, B. Zhu, J. Yu, J. Xu, $CuInS_2$ sensitized TiO_2 hybrid nanofibers for improved photocatalytic CO_2 reduction, Appl. Catal. B Environ. 23 (2018) 194–202, https://doi.org/10.1016/j.apcatb.2018.02.042.
[22] R. Wang, X. Tong, A.I. Channa, Q. Zeng, J. Sun, C. Liu, X. Li, J. Xu, F. Lin, G. S. Selopal, F. Rosei, Y. Zhang, J. Wu, H. Zhao, A. Vomiero, X. Sun, Z.M. Wang, Environmentally friendly Mn-alloyed core/shell quantum dots for high-efficiency photoelectrochemical cells, J. Mater. Chem. A 8 (2020) 10736–10741, https://doi.org/10.1039/D0TA00953A.
[23] W. Yang, Y. Oh, J. Kim, M.J. Jeong, J.H. Park, J. Moon, Molecular chemistry-controlled hybrid ink-derived efficient Cu_2ZnSnS_4 photocathodes for photoelectrochemical water splitting, ACS Energy Lett. 1 (2016) 1127–1136, https://doi.org/10.1021/acsenergylett.6b00453.
[24] F. Ozel, E. Aslan, B. Istanbullu, O. Akay, I.H. Patir, Photocatalytic hydrogen evolution based on Cu_2ZnSnS_4, Cu_2NiSnS_4 and Cu_2CoSnS_4 nanocrystals, Appl. Catal. B Environ. 198 (2016) 67–73, https://doi.org/10.1016/j.apcatb.2016.05.053.
[25] L. Yu, R.S. Kokenyesi, D.A. Keszler, A. Zunger, Inverse design of high absorption thin-film photovoltaic materials, Adv. Energy Mater. 3 (2013) 43–48, https://doi.org/10.1002/aenm.201200538.
[26] T. Ohno, M. Akiyoshi, T. Umebayashi, K. Asai, T. Mitsui, M. Matsumura, Preparation of S-doped TiO_2 photocatalysts and their photocatalytic activities under visible light, Appl. Catal. A 265 (2004) 115–121, https://doi.org/10.1016/j.apcata.2004.01.007.
[27] N. Mufti, T. Amrillah, A. Taufiq, Sunaryono, M. Aripriharta, M. Diantoro, Zulhadjri, H. Nur, Review of CIGS-based solar cells manufacturing by structural engineering, Sol. Energy 207 (2020) 1146–1157, https://doi.org/10.1016/j.solener.2020.07.065.
[28] T.J. Whittles, T.D. Veal, C.N. Savory, P.J. Yates, P.A.E. Murgatroyd, J.T. Gibbon, M. Birkett, R.J. Potter, J.D. Major, K. Durose, D.O. Scanlon, V.R. Dhanak, Band alignments, band gap, core levels, and valence band states in Cu_3BiS_3 for photovoltaics, ACS Appl. Mater. Interfaces 11 (2019) 27033–27047, https://doi.org/10.1021/acsami.9b04268.
[29] J. Li, Y. Zhao, X. Han, D. Xiao, A facile strategy for fabricating particle-on-flower Au-Cu_3BiS_3 nanostructures for enhanced photoelectrocatalytic activity in water splitting, New J. Chem. 45 (2021) 1231–1239, https://doi.org/10.1039/D0NJ03448G.
[30] S. Kamimura, N. Beppu, Y. Sasaki, T. Tsubota, T. Ohno, Platinum and indium sulfide-modified Cu_3BiS_3 photocathode for photoelectrochemical hydrogen evolution, J. Mater. Chem. A 5 (2017) 10450–10456, https://doi.org/10.1039/C7TA02740K.
[31] J.K. Nørskov, J. Rossmeisl, A. Logadottir, L. Lindqvist, Origin of the overpotential for oxygen reduction at a fuel-cell cathode, J. Phys. Chem. B 108 (2004) 17886–17892, https://doi.org/10.1021/jp047349j.
[32] B. Dong, Y. Qi, J. Cui, B. Liu, F. Xiong, X. Jiang, Z. Li, Y. Xiao, F. Zhang, C. Li, Synthesis of $BaTaO_2N$ oxynitride from Ba-rich oxide precursor for construction of visible-light-driven Z-scheme overall water splitting, Dalton Trans. 46 (2017) 10707–10713, https://doi.org/10.1039/C7DT00854F.
[33] J. Wang, Y. Song, J. Hu, Y. Li, Z. Wang, P. Yang, G. Wang, Q. Ma, Q. Che, Y. Dai, B. Huang, Photocatalytic hydrogen evolution on p-type tetragonal zircon $BiVO_4$, Appl. Catal. B Environ. 251 (2019) 94–101, https://doi.org/10.1016/j.apcatb.2019.03.049.
[34] J. Zheng, Z. Lei, Incorporation of CoO nanoparticles in 3D marigold flower-like hierarchical architecture $MnCo_2O_4$ for highly boosting solar light photo-oxidation and reduction ability, Appl. Catal. B Environ. 237 (2018) 1–8, https://doi.org/10.1016/j.apcatb.2018.05.060.

[35] S. Xu, N. Cheng, H. Yin, D. Cao, B. Mi, Electrospray preparation of $CuInS_2$ films as efficient counter electrode for dye-sensitized solar cells, Chem. Eng. J. 397 (2020) 1385–8947, https://doi.org/10.1016/j.cej.2020.125463.
[36] H. Deng, X. Fei, Y. Yang, J. Fan, J. Yu, B. Cheng, L. Zhang, S-scheme heterojunction based on p-type $ZnMn_2O_4$ and n-type ZnO with improved photocatalytic CO_2 reduction activity, Chem. Eng. J. 409 (2021), 127377, https://doi.org/10.1016/j.cej.2020.127377.
[37] J. Leng, Z. Wang, J. Wang, H. Wu, G. Yan, X. Li, H. Guo, Y. Liu, Q. Zhang, Z. Guo, Advances in nanostructures fabricated via spray pyrolysis and their applications in energy storage and conversion, Chem. Soc. Rev. 48 (2019) 3015–3072, https://doi.org/10.1039/C8CS00904J.
[38] Y. Li, H.L. Wang, L.M. Xie, Y.Y. Liang, G.S. Hong, H.J. Dai, MoS_2 nanoparticles grown on graphene: an advanced catalyst for the hydrogen evolution reaction, J. Am. Chem. Soc. 133 (2011) 7296–7299, https://doi.org/10.1021/ja201269b.
[39] S. Yang, K. Liu, W. Han, L. Li, F. Wang, X. Zhou, H. Li, T. Zhai, Salt-assisted growth of p-type Cu_9S_5 nanoflakes for p-n heterojunction photodetectors with high responsivity, Adv. Funct. Mater. 30 (2019), 1908382, https://doi.org/10.1002/adfm.201908382.
[40] S. Kamimura, Y. Sasaki, M. Kanaya, T. Tsubota, T. Ohno, Improvement of selectivity for CO_2 reduction by using Cu_2ZnSnS_4 electrodes modified with different buffer layers (CdS and In_2S_3) under visible light irradiation, RSC Adv. 6 (2016) 112594–112601, https://doi.org/10.1039/C6RA22546B.
[41] W. Tang, H. Lin, A. Kleiman-Shwarsctein, G.D. Stucky, E.W. McFarland, Size-dependent activity of gold nanoparticles for oxygen electroreduction in alkaline electrolyte, J. Phys. Chem. C 112 (2008) 10515–10519, https://doi.org/10.1021/jp710929n.
[42] L. Li, Z. Hu, J.C. Yu, On-demand synthesis of H_2O_2 by water oxidation for sustainable resource production and organic pollutant degradation, Angew. Chem. Int. Ed. 59 (2020) 20538–20544, https://doi.org/10.1002/ange.202008031.
[43] J. Sun, Y. Yu, A.E. Curtze, X. Liang, Y. Wu, Dye-sensitized photocathodes for oxygen reduction: efficient H_2O_2 production and aprotic redox reactions, Chem. Sci. 10 (2019) 5519–5527, https://doi.org/10.1039/C9SC01626K.
[44] W. Fan, B. Zhang, X. Wang, W. Ma, D. Li, Z. Wang, M. Dupuis, J. Shi, S. Liao, C. Li, Efficient hydrogen peroxide synthesis by metal-free polyterthiophene via photoelectrocatalytic dioxygen reduction, Energy Environ. Sci. 13 (2020) 238–245, https://doi.org/10.1039/C9EE02247C.
[45] J. Sun, Y. Wu, Anthraquinone redox relay for dye-sensitized photo-electrochemical H_2O_2 production, Angew. Chem. Int. Ed. 59 (2020) 10904–10908, https://doi.org/10.1002/anie.202003745.
[46] L. Migliaccio, M. Gryszel, V. Đerek, A. Pezzella, E.D. Głowacki, Aqueous photo (electro)catalysis with eumelanin thin films, Mater. Horiz. 5 (2018) 984–990, https://doi.org/10.1039/C8MH00715B.
[47] O. Jung, M.L. Pegis, Z. Wang, G. Banerjee, C.T. Nemes, W.L. Hoffeditz, J.T. Hupp, C.A. Schmuttenmaer, G.W. Brudvig, J.M. Mayer, Highly active NiO photocathodes for H_2O_2 production enabled via outer-sphere electron transfer, J. Am. Chem. Soc. 140 (2018) 4079–4084, https://doi.org/10.1021/jacs.8b00015.